Journal of Materials Chemistry A

COMMUNICATION

View Article Online
View Journal | View Issue

Cite this: *J. Mater. Chem. A*, 2025, **13**, 7073

Received 18th January 2025
Accepted 17th February 2025

DOI: 10.1039/d5ta00494b

rsc.li/materials-a

Structured droplets dominated by interfacial self-assembly of topology-tunable Janus particles towards macroscopic materials†

Wenzhong Zhai, ‡[a] Xubo Liu,‡[a] Jiajia Zhou, ‡[c] Qi Yu,[a] Miao Liu,[d] Jingxin Meng, [a] Lu Zhang,[d] Jun-Bing Fan *[b] and Shutao Wang *[a]

Structured droplets, constructed and stabilized by interfacial self-assembly and jamming of colloidal particles, have shown potential applications in biphasic reactors towards fabrication of functional materials. However, the fabrication of macroscopic granular materials using structured droplets remains a great challenge due to the instability of colloidal particle assemblies at the macroscale droplet interface and the coalescence between droplets. Herein, we demonstrate a distinctly interfacial self-assembly of topology-tunable Janus particles (including bread, hemisphere and crescent) at the macro-droplet interface, enabling the fabrication of stably structured droplets with a solid-like membrane and thereby greatly affording the downstream production of macroscopic granular materials. The self-assembly towards the fabrication of structured droplets is attributed to the interfacial desorption energy difference triggered by Janus particle topologies. Only hemispherical Janus particles could perform fully interfacial jamming, thereby forming the robust structured droplets. These Janus particle-dominated structured droplets as a biphasic reactor can be used to controllably produce macroscopic granular materials with tunable sizes and functionalities. This study will widen the applications of the interfacial self-assembly from the microscale to the macroscale towards the fabrication of functional materials.

Introduction

The self-assembly of colloidal particles at oil–water interfaces has been considered one of the most powerful strategies to construct structured liquids,[1–3] complex superstructures[4–6] and functional materials.[7–9] In general, colloidal particles self-assemble and jam at the interface, resulting in a phase transition of the self-assembly from "liquid-like" to "solid-like".[10–14] The resulting "solid-like" soft materials with robust mechanical properties would endow the liquids with controllable structures from spherical shapes to non-equilibrium ellipsoidal shapes, known as structured droplets.[15–18] These droplets have shown potential applications in biphasic reactors,[15] embolic materials[17] and all-liquid devices.[18] The majority of interfacial assemblies for the fabrication of structured droplets have been achieved *via* spherical nanoparticles.[1,19] However, the reduction of interfacial energy driven by particles on the nanoscale is much smaller due to the low desorption energy, leading to an unstable assembly of nanoparticles at the oil–water interface. Nanoscale particle surfactants easily eject from the interface compared with large microscale particles, making it difficult to fabricate stably structured droplets, especially macro-scale droplets, due to the instant coalescence at the millimeter-scale curvature radius.[20–23]

Colloidal particle-stabilized pH-responsive emulsions and Pickering emulsion-based synthesis have been widely studied from the nanoscale to the microscale.[24–29] It is a great challenge to synthesize functional macroscopic granular materials within macroscale biphasic droplet reactors, considering the interfacial stability and structures of emulsified droplets which are dominated by the colloidal particle surfactants assembled at the water–oil interface. Recently, B. Haney *et al.* successfully obtained millimeter-sized emulsion droplets, but with a non-ideal wide distribution of diameters. And these emulsion droplets were interfacially unstable due to the sub-millimeter sized amphiphilic Janus spheres (with diameters of 100–500 μm), leading to obvious coalescence.[28] The key point to stabilize macro-droplets is making the particle surfactants firmly

[a]*CAS Key Laboratory of Bio-inspired Materials and Interfacial Science, CAS Center for Excellence in Nanoscience, Technical Institute of Physics and Chemistry, Chinese Academy of Sciences, Beijing 100190, P. R. China. E-mail: stwang@mail.ipc.ac.cn*

[b]*. Cancer Research Institute, Experimental Education/Administration Center, School of Basic Medical Sciences, Southern Medical University, Guangzhou 510515, P. R. China. E-mail: fjb2012@mail.ipc.ac.cn*

[c]*South China Advanced Institute for Soft Matter Science and Technology, School of Emergent Soft Matter, South China University of Technology, Guangzhou 510515, P. R. China*

[d]*Key Laboratory of Photochemical Conversion and Optoelectronic Materials, Technical Institute of Physics and Chemistry, Chinese Academy of Sciences, Beijing 100190, P. R. China*

† Electronic supplementary information (ESI) available. See DOI: https://doi.org/10.1039/d5ta00494b

‡ W. Z., X. L., and J. Z. contributed equally to this work.

absorbed at the oil/water interface by increasing their surfactancy, *e.g.*, optimizing the topologies and chemical functionalities.

When a colloidal particle assembles at the oil–water interface, the change in interfacial energy (ΔG) is the main driving force for its assembly, which is highly dependent on the size and contact angle of particles.[30,31]

$$\Delta G = -\pi r^2 \gamma_{o/w} (1 - |\cos\theta|)^2 \quad (1)$$

where r is the radius of the particle, $\gamma_{o/w}$ is interfacial tension of the oil–water interface, and θ is the contact angle of the particle at the interface.

From eqn (1), we can clearly see that the reduction of interfacial energy is proportional to the r^2 of the particle. That is, micro-sized particles would be more efficient than nano-sized particles due to the decrease in the interfacial energy, resulting in an effective confinement into the interface. Thus, to achieve good stability of structured droplets, rationally designing colloidal particles with as large a size as possible and neutral wetting properties (with the contact angle approaching 90°) is essential.[30]

Herein, we demonstrate that Janus particles with tunable topologies (including bread, hemisphere and crescent) and an average diameter larger than 2 μm show different interfacial assembly dynamics at the macro-scale droplet interface. The self-assembly is highly dependent on the topologies of Janus particles, and only hemispherical Janus particles can fully cover the whole water–oil interface at a certain concentration, enabling the formation of structured millimeter-sized droplets and downstream fabrication of macroscopic materials. These Janus particle-dominated structured droplets exhibit great potential in biphasic reactors, enabling the monomer polymerization to fabricate functional macroscopic granular materials.

Results and discussion

The synthesis of Janus particles was performed by our previously reported emulsion interfacial polymerization strategy.[32–34] Their topologies could be precisely controlled from bread-shaped and hemisphere-shaped to crescent-shaped in order by merely tuning the feed amounts of the swelling agent (1-chlorodecane) (Fig. 1a–c and S1a–c, ESI†). The synthetic Janus particles were composed of a hydrophobic poly(styrene-*co*-divinylbenzene) (PSDVB) bulk and hydrophilic poly (acrylic acid) (PAA) layer.[33] The sizes of bread-shaped Janus particles, hemisphere-shaped Janus particles and crescent-shaped Janus particles were 2.2 ± 0.2 μm, 2.2 ± 0.1 μm and 2.3 ± 0.2 μm, respectively, and they exhibited excellent uniformity and similar zeta potentials (∼−27 mV, Fig. S1d, ESI†). The three-phase contact angles of bread-shaped Janus particles, hemispherical Janus particles and crescent-shaped Janus particles were 85.3 ± 3.1°, 90.3 ± 2.3° to 97.6 ± 4.6°, respectively (Fig. S2, ESI†). We first investigated the dynamic self-assembly behaviors of these Janus particles towards the fabrication of structured droplets at the oil–water interface by the pendant drop method with an oscillating tensiometer. A water droplet (8 μL) containing Janus particles (5 mg mL^{-1}) was immerged into a decane phase and then was periodically expanded and compressed at a set frequency (Fig. 1d and Movie S1, ESI†). We observed that Janus particles could assemble along the water–decane interface and only hemispherical Janus particles were able to continually assemble until fully covering the whole interface to allow the fabrication of a structured droplet with a solid-like membrane, while the bread-shaped and crescent-shaped Janus particles could assemble only on small portions of the interfaces (Fig. 1e–h), and the surface coverages of bread-shaped and crescent-shaped Janus particle-dominated droplets were less than 40%. The results demonstrated that the interfacial self-assembly of these Janus particles towards the fabrication of structured droplets is highly dependent on their topologies.

To investigate the mechanism of Janus particle topology-manipulated self-assembly for the fabrication of structured droplets with a solid-like membrane, we first calculated the desorption energy (ΔG) of a Janus particle (Fig. 2a).[35–38] The ΔG is defined as the free energy required for the Janus particle to desorb from the oil–water interface into the water phase, $\Delta G = G_{water} - G_{interface}$. For bread-shaped Janus particles, topology can be approximated to the shape of a sphere that is cut at a half-angle θ_0. For hemispherical Janus particles, θ_0 is $\pi/2$. Thus, for bread-shaped Janus particles, we have

$$G_{water} = 2\pi r^2(1 + \cos\theta_0)\gamma_{water-PAA} + \pi r^2 \sin^2\theta_0\gamma_{water-PS} + \pi r^2\sin^2\theta_0\gamma_{water-oil} \quad (2)$$

$$G_{interface} = 2\pi r^2(1 + \cos\theta_0)\gamma_{water-PAA} + \pi r^2 \sin^2\theta_0\gamma_{oil-PS} \quad (3)$$

Here we assume that the three-phase contact line between the Janus particle and the water–oil interface lies rightly on the PS–PAA boundary.

The desorption energy for bread-shaped Janus particles is

$$\Delta G_{bread} = \pi r^2 \sin^2\theta_0(\gamma_{water-PS} - \gamma_{oil-PS} + \gamma_{water-oil}) > 0 \quad (4)$$

The ΔG_{bread} is greater than zero, indicating that the Janus particle tends to stay at the interface. From eqn (4), the desorption energy of a hemispherical Janus particle ($\theta_0 = \pi/2$) should be greater than that of a bread-shaped Janus particle ($\theta_0 < \pi/2$). The hemispherical Janus particle shows a higher surfactancy than the bread-shaped Janus particle.

For crescent-shaped Janus particles, we have

$$G_{water} = 2\pi r^2(1 + \cos\theta_0)\gamma_{water-PAA} + S\gamma_{water-PS} + \pi r^2 \sin^2\theta_0\gamma_{water-oil} \quad (5)$$

$$G_{interface} = 2\pi r^2(1 + \cos\theta_0)\gamma_{water-PAA} + S\gamma_{oil-PS} \quad (6)$$

The concaved PSDVB surface area is defined as S. We assume that the concave surface is in contact with the oil phase. The desorption energy for crescent-shaped Janus particles is

$$\Delta G_{crescent} = S(\gamma_{water-PS} - \gamma_{oil-PS}) + \pi r^2 \sin^2\theta_0\gamma_{water-oil} \quad (7)$$

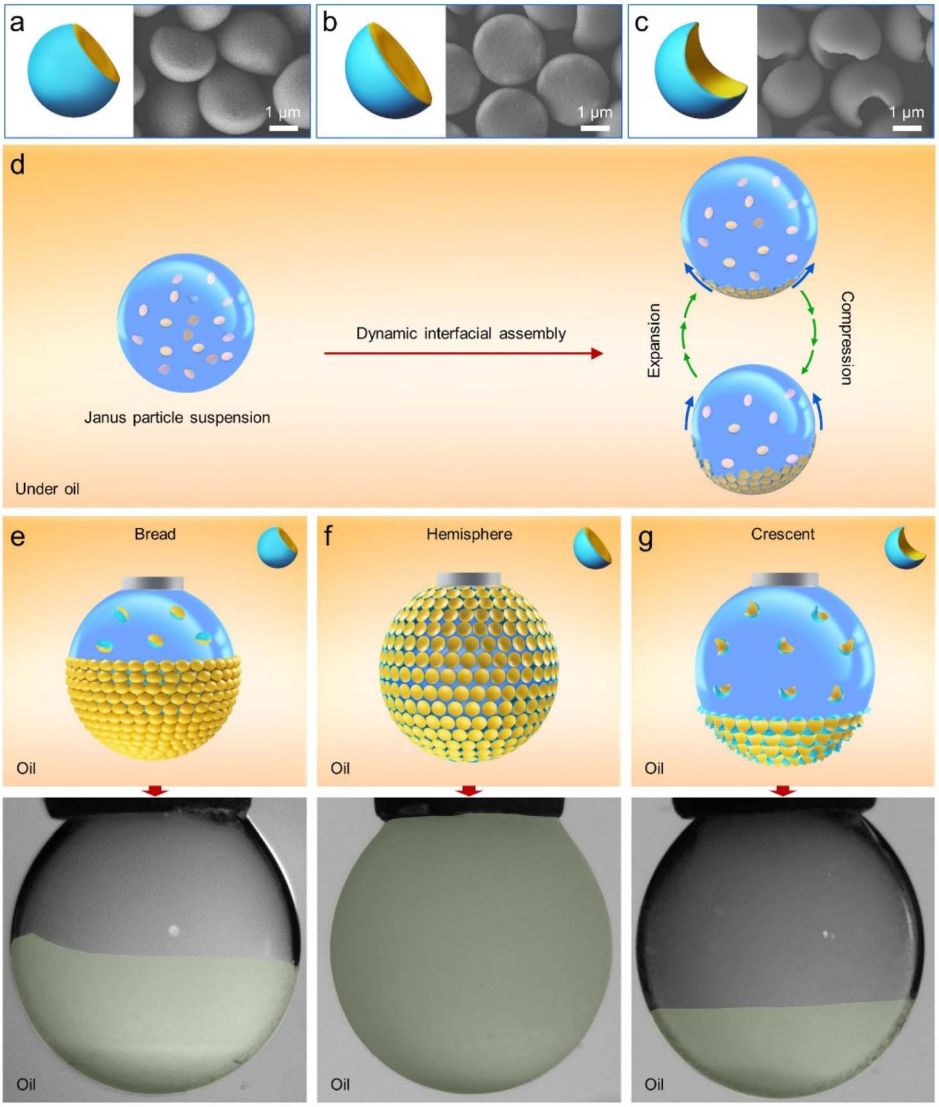

Fig. 1 Structured droplets dominated by the interfacial self-assembly of topology-tunable Janus particles. (a–c) Schematics and scanning electron microscope (SEM) images of Janus particles. Three kinds of Janus particles were controllably fabricated, including bread, hemisphere, and crescent shapes. Their chemical compositions were hydrophobic poly(styrene-*co*-divinylbenzene) (PSDVB) bulk and hydrophilic poly (acrylic acid) (PAA) layer. (d–g) The topology-tunable Janus particle-dominated interfacial self-assembly. A water droplet containing Janus particles was immerged into a decane phase and then was periodically expanded and compressed. Interestingly, only hemispherical Janus particles continually self-assembled until fully covering the whole macro-droplet interface to allow the fabrication of a structured droplet with a solid-like membrane, while bread-shaped and crescent-shaped Janus particles could assemble into the interfaces with less than 40% surface coverage.

Since $\gamma_{water-PS} - \gamma_{oil-PS} > 0$ and $\Delta G_{crescent}$ is proportional to S, surface coverage of the assembled crescent-shaped Janus particle should be larger than that of the bread-shaped Janus particle when the oil phase completely covers the PSDVB surface. It is not clear yet whether the oil phase will fully cover the hydrophobic PSDVB surface for the crescent-shaped Janus particles. To verify, we used a gel-trapping technique[32] to directly visualize the adsorption and orientation of these Janus particles at the water–oil interface. The aqueous solution of Janus particles (1 mg mL^{-1}) was slowly injected close to the interface of decane and Gellan gel aqueous solution at 50 °C. After attaching to the interface, the Janus particles were then trapped in Gellan gel cooled at room temperature and then transferred to a PDMS matrix. In this process, the hydrophobic PSDVB side confronts PDMS, while the hydrophilic PAA layer faces water. As shown in Fig. 2b–d and S2a–c (ESI),† only two tip sections of crescent-shaped Janus particles were covered by the oil phase (Fig. 2d). For the bread-shaped Janus particles and hemispherical Janus particles, hydrophobic PSDVB surfaces were fully covered with the oil phase (Fig. 2b and c). These results suggested that crescent-shaped Janus particles should be more difficult to adsorb into the interface than bread-shaped Janus particles and hemispherical Janus particles, probably due to their rigid topologies. Thus, desorption energy (ΔG.) for these

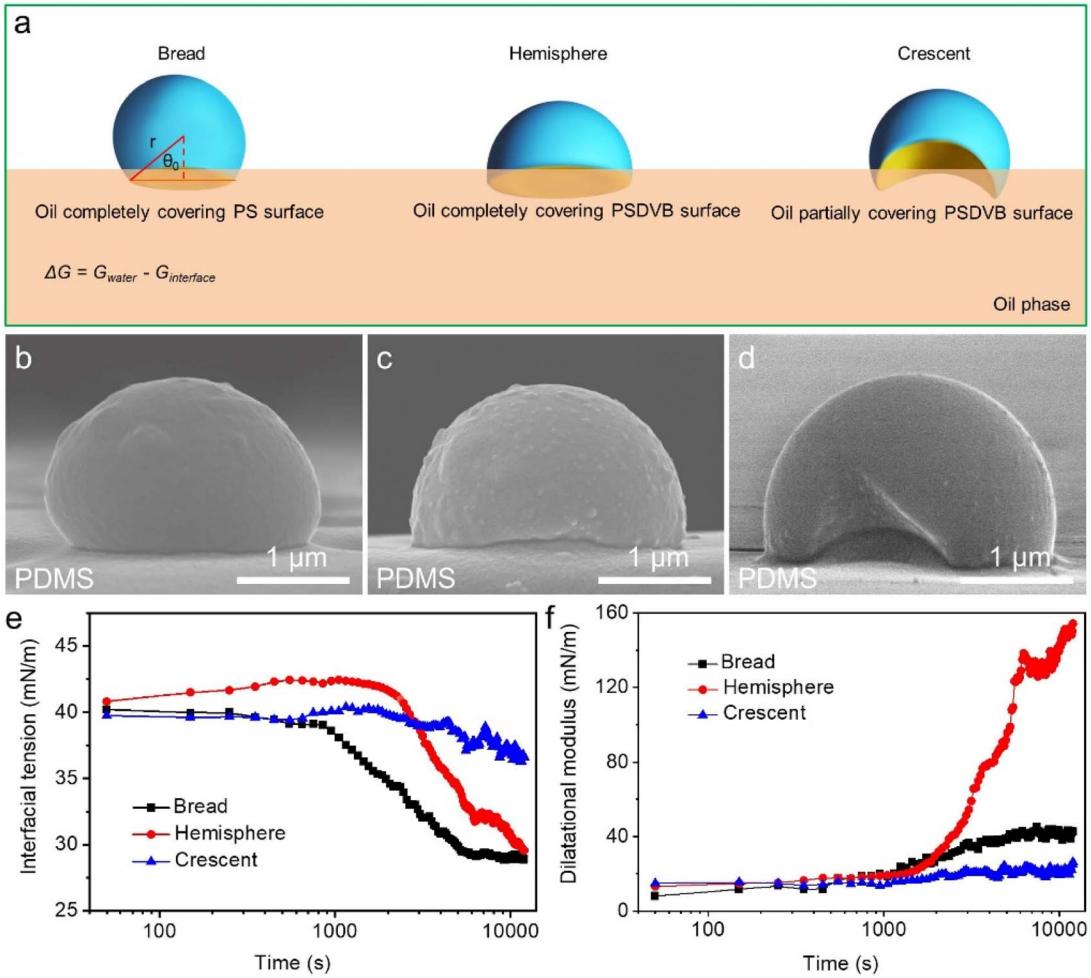

Fig. 2 The mechanism of Janus particle topology-dominated interfacial self-assembly for the fabrication of structured droplets with solid-like membranes. (a–d) Schematics and SEM images of the interfacial adsorption behaviors of the three kinds of Janus particles. The self-assembly of these Janus particles towards the fabrication of structured droplets with a solid-like membrane is highly dependent on their topologies, into which the difference in desorption energy (ΔG) plays a critical role. For the bread-shaped Janus particles and hemispherical Janus particles, their hydrophobic PSDVB surfaces were fully covered with the oil phase (PDMS). By contrast, for the crescent-shaped Janus particles, only partial regions (two tip sections) of the PSDVB surface were covered with the oil phase. (e) Interfacial tension *vs.* time during the self-assembly process of Janus particles. (f) Dilatational modulus *vs.* time during the self-assembly process of Janus particles. The dilatational modulus of the obtained solid-like membrane by hemispherical Janus particles went up to 154 mN m^{-1}, which was much higher than those of bread-shaped Janus particles (42 mN m^{-1}) and crescent-shaped Janus particles (26 mN m^{-1}).

Janus particles should be $\Delta G_{\text{hemisphere}} > \Delta G_{\text{bread}} > \Delta G_{\text{crescent}}$, accordingly. Bread-shaped Janus particles and hemispherical Janus particles reduced the interfacial tension from ~40 mN m^{-1} to ~28 mN m^{-1}, while crescent-shaped Janus particles with lower surfactancy reduced interfacial tension from ~40 mN m^{-1} to ~37 mN m^{-1} within 3 h (Fig. 2e). The rigidity and toughness of the solid-like membranes at droplet interfaces were then measured on their surface dilatational modulus. The dilatational modulus of the obtained solid-like membrane assembled using hemispherical Janus particles went up to 154 mN m^{-1}, which was much higher than those of bread-shaped Janus particles (42 mN m^{-1}) and crescent-shaped Janus particles (26 mN m^{-1}) (Fig. 2f). Therefore, the hemispherical Janus particles form densely packed assemblies easier than bread-shaped Janus particles and crescent-shaped Janus particles, enabling the fabrication of ellipsoidal structured droplets with tough and elastic membranes at the macro-droplet interface.

We next carefully observed the fabrication process of Janus particle-dominated structured droplets at different times. In the beginning, Janus particles dispersed randomly with Brownian motion inside the droplet. Once absorbed onto the water–oil interface, Janus particle (with a diameter of ~2.2 μm) assemblies aggregated and subsequently deposited along the droplet surface under the gravity effect. The water–oil interface was fully covered at ~110 min, and the interfacial absorption equilibrium was reached at ~178 min, forming a solid-like particle membrane (Fig. 3a). There are two possible factors affecting the assembly of the hemispherical particles. (1) The diffusion coefficient D_0 of the Janus particles. A randomly dispersed micro-scaled Janus particle diffused from the bulk phase to the

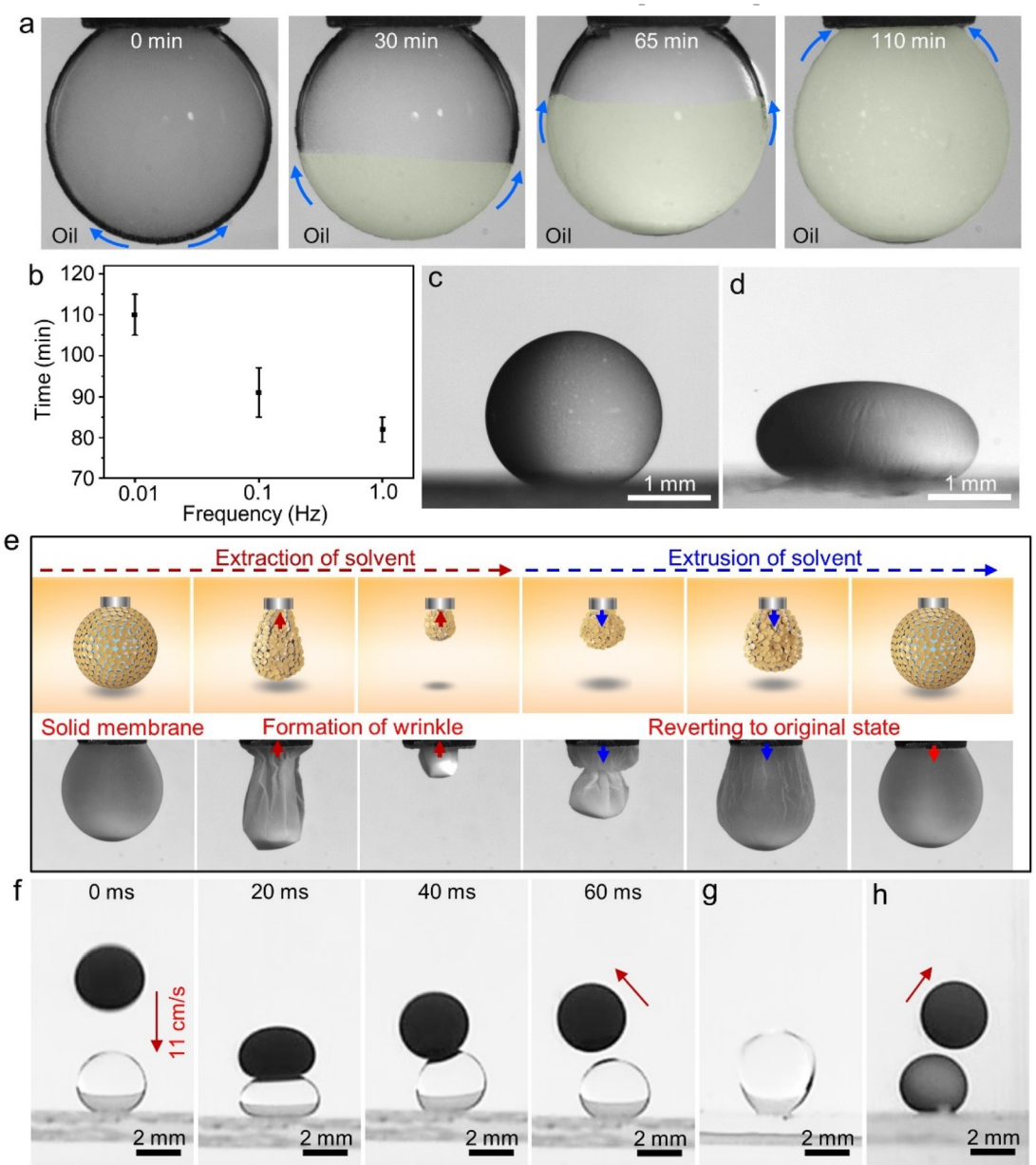

Fig. 3 The time-dependent self-assembly and stability of Janus particle-dominated structured droplets. (a) The time-dependent self-assembly process of hemispherical Janus particles. Starting from the bottom of the droplet interface, hemispherical Janus particles enabled self-assembly to form structured droplets with a solid-like membrane. (b) The self-assembly time for the fabrication of structured droplets with a solid-like membrane could be controlled by regulating the frequencies of expansion and compression. (c–e) Janus particle-dominated structured droplets. (c and d) The obtained structured droplets exhibited excellent elasticity and could be deformed into an ellipsoid by an external pressure. (e) The solid-like membrane of the structured droplets could largely bend or wrinkle when extracting water from the droplet and stretch back to the origin when reinjecting water into the droplet reversibly. (f–h) Snapshots of the collision process between two droplets under oil. (f) Janus particle-dominated structured droplets collided with a pure water droplet, and it was ejected from the surface. (g) A pure water droplet collided with a pure water droplet, and they were coalesced together. (h) The collision between two Janus particle-dominated structured droplets, and one was ejected from the surface.

water–oil interface, where thermal dynamics of the particle was determined from the diffusion coefficient D_0. According to the Stokes–Einstein equation,[39,40] $D_0 = k_B T/6\pi\eta r$, where r is the radius of the particle, η is the viscosity of the solution, and $k_B T$ is the thermal energy of the particle. Our micro-scaled Janus particles with a larger radius may have a lower diffusion coefficient in the bulk compared with nanoparticles or molecular surfactants, limiting and slowing down the interfacial assembly. (2) The frequency of repeated expansion and compression of pendant droplets. As shown in Fig. 3b, the self-assembly time for the fabrication of structured droplets could be reduced from ~110 min to ~80 min obviously when the frequencies of repeated expansion and compression of pendant droplets were increased from 0.01 Hz to 1.0 Hz. This indicates

that interfacial mechanical perturbations induce rapid deformation and Marangoni flow fields at the water–oil interface, effectively accelerating particle migration and lateral rearrangement. Moreover, we found that when the concentrations of Janus particles were equal to or greater than 5 mg mL^{-1}, hemispherical Janus particles were enabled to assemble at the droplet interface (volume of 8 μL) for the fabrication of structured droplets (Fig. S3b, ESI†). Accordingly, the interfacial tension was gradually reduced with the increase of concentrations of Janus particles (Fig. S4, ESI†). In contrast, the structured droplets with a solid-like membrane remained unable to be fabricated in the bread-shaped Janus particle- or crescent-shaped Janus particle-dominated self-assembly, even at 10 mg mL^{-1} of concentration (Fig. S3a and c, ESI†). Millimeter-sized droplets could be constructed and stabilized even at large volumes from 2 μL to 25 μL (Fig. S5, ESI†).

We comprehensively investigated the stability of the obtained structured droplets. As shown in Fig. 3c and d, a hemispherical Janus particle-dominated spherical droplet could be deformed into an ellipsoid using an external mechanical stimulus. After removing the external stress, the ellipsoidal droplet was immediately "locked-in" by interfacial rearrangement of the Janus particles. The structured droplets with solid-like membranes could largely bend or wrinkle when extracting the liquid and be stretched back to the original morphologies after reinjecting the liquid reversibly (Fig. 3e and Movie S2, ESI†). During this process, hemispherical Janus particles exhibited excellent adsorption capacity and they could neither move laterally nor be ejected off the water–decane interface even when being largely compressed due to the high desorption energy and strong jamming effect. Moreover, the obtained structured droplets enabled prevention of the coalescence of water droplets effectively, even after a fierce

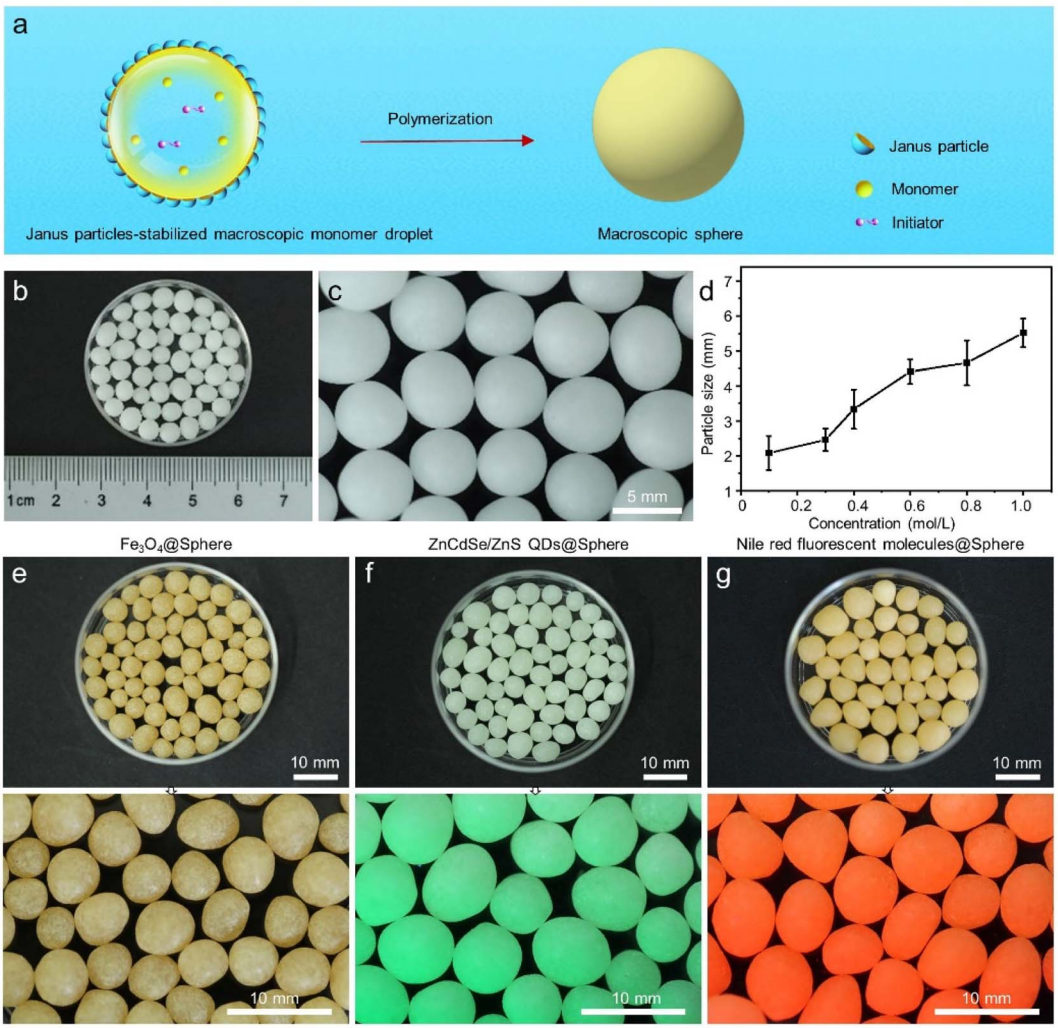

Fig. 4 Janus particle-dominated structured droplets for the fabrication of macroscopic granular materials. (a) Schematic of the fabrication of macroscopic granular materials. When the oil phase was a polymeric monomer, such as styrene, styrene-in-water droplets could be fabricated by using hemispherical Janus particles as stabilizers. After polymerizing these structured droplets, macroscopic materials could be fabricated. (b and c) Photographs of the obtained macroscopic materials. (d) The sizes of the macroscopic granular materials could be controlled by tuning the concentrations of the monomer. (e–g) Photographs of the obtained functional macroscopic materials. When introducing the magnetic Fe_3O_4 nanoparticles, ZnCdSe/ZnS quantum dots or Nile red fluorescent molecules into the styrene-in-water structured droplets, the polymerization enabled production of magnetic macroscopic materials or fluorescent macroscopic materials.

collision with a falling speed of 11 cm s^{-1} (Fig. 3f). By contrast, pure water droplets completely merged (Fig. 3g and S6a, ESI†). When one structured droplet with a solid-like membrane was collided with another one, it could bounce away under oil (Fig. 3h and S6b, ESI†). These results demonstrated that Janus particle-dominated structured droplets with a robust solid-like membrane have excellent stability, which could provide a stable biphasic droplet reactor for the synthesis of macroscopic materials on the millimeter scale or even larger.

Finally, we demonstrated the application of these Janus particle-dominated structured droplets to produce macroscopic materials. Currently, macroscopic granular materials have been widely used in industry. However, millimeter sized emulsion droplets were usually unstable at the interface due to the low packing density or small desorption energy of the absorbed amphiphilic Janus spheres.[28] And they are usually fabricated by material processing (involving mixing, molding, and post-processing) *via* giant machines,[41,42] leading to a sophisticated preparation process, large occupation area, and high energy consumption and cost. Herein, we could produce macroscopic materials by using Janus particle-dominated structured droplets as biphasic reactors. As shown in Fig. 4a, when the oil phase was replaced with a polymeric monomer, such as styrene, we could produce styrene-in-water structured droplets using hemispherical Janus particles. After polymerizing these structured droplets, macroscopic materials could be fabricated (Fig. 4a–c). The sizes of the macroscopic granular materials could be controlled from 2.1 ± 0.5 mm to 5.5 ± 0.4 mm by tuning the concentrations of the monomer. After polymerization, these Janus particles could be recycled by treating the macroscopic particle solutions with ultrasound (Fig. S7, ESI†). To demonstrate the effectiveness of this strategy, we could also fabricate functional macroscopic materials. As shown in Fig. 4e–g, when introducing the magnetic Fe_3O_4 nanoparticles or quantum dots into the styrene-in-water structured droplets, the polymerization enabled the production of magnetic or fluorescent macroscopic granular materials.

Conclusions

In summary, we have demonstrated the interfacial self-assembly dynamics of topology-tunable Janus particles with bread, hemispherical and crescent morphologies respectively. The interfacial self-assembly and jamming of hemispherical Janus particles at the water–decane interface allows the formation of controllably structured droplets with robust solid-like membranes. The Janus particle-dominated structured droplets exhibit excellent elasticity and strength, possessing the properties to withstand large bending and fierce collision. These millimeter-sized droplets can be further used as reactors to produce macroscopic granular materials with tunable sizes and functionalities, *e.g.*, modified with magnetic or fluorescent properties, inspiring applications in biomedical encapsulation and fluorescent indicators.

Data availability

The data that support the findings of this study are available from the corresponding author upon reasonable request.

Conflicts of interest

The authors declare no conflicts of interest.

Acknowledgements

The authors acknowledge the financial support from the National Natural Science Foundation (21872158, 22075127, 21875269 and 21972155) and National Key R&D Program of China (2019YFA0709302 and 2020YFA0710403).

References

1 A. Ghaffarkhah, S. A. Hashemi, A. A. Isari, M. Panahi-Sarmad, F. Jiang, T. P. Russell, O. J. Rojas and M. Arjmand, *Chem. Soc. Rev.*, 2024, **53**, 9652–9717.
2 X. Liu, N. Kent, A. Ceballos, R. Streubel, Y. Jiang, Y. Chai, P. Y. Kim, J. Forth, F. Hellman, S. Shi, D. Wang, B. A. Helms, P. D. Ashby, P. Fischer and T. P. Russell, *Science*, 2019, **365**, 264–267.
3 Y. Yang, H. Sun, M. Wang, M. Li, Z. Zhang, T. P. Russell and S. Shi, *Angew. Chem., Int. Ed.*, 2023, **62**, e202218440.
4 A. D. Dinsmore, M. F. Hsu, M. G. Nikolaides, M. Marquez, A. R. Bausch and D. A. Weitz, *Science*, 2002, **298**, 1006–1009.
5 S. Hou, L. Bai, D. Lu and H. Duan, *Acc. Chem. Res.*, 2023, **56**, 740–751.
6 F. Grillo, M. A. Fernandez-Rodriguez, M. N. Antonopoulou, D. Gerber and L. Isa, *Nature*, 2020, **582**, 219–224.
7 S. Crossley, J. Faria, M. Shen and D. E. Resasco, *Science*, 2010, **327**, 68–72.
8 M. Zhang, R. Ettelaie, T. Li, J. Yang, L. Dong, N. Xue, B. P. Binks, F. Cheng and H. Yang, *Nat. Catal.*, 2024, **7**, 295–306.
9 Z. Li, Q. Fan and Y. Yin, *Chem. Rev.*, 2022, **122**, 4976–5067.
10 P. Aussillous and D. Quéré, *Nature*, 2001, **411**, 924–927.
11 K. Stratford, R. Adhikari, I. Pagonabarraga, J. C. Desplat and M. E. Cates, *Science*, 2005, **309**, 2198–2201.
12 M. Tenjimbayashi and R. Tamate, *J. Mater. Chem. A*, 2024, **12**, 16343–16349.
13 C. Huang, J. Forth, W. Wang, K. Hong, G. S. Smith, B. A. Helms and T. P. Russell, *Nat. Nanotechnol.*, 2017, **12**, 1060–1063.
14 B. Wu, C. Yang, Q. Xin, L. Kong, M. Eggersdorfer, J. Ruan, P. Zhao, J. Shan, K. Liu, D. Chen, D. A. Weitz and X. Gao, *Adv. Mater.*, 2021, **33**, 2102362.
15 M. Cui, T. Emrick and T. P. Russell, *Science*, 2013, **342**, 460–463.
16 F. Yan, L. Hu, Z. Ji, Y. Lyu, S. Chen, L. Xu and J. Hao, *Angew. Chem., Int. Ed.*, 2024, **63**, e202318926.
17 S. Tao, B. Lin, H. Zhou, S. Sha, X. Hao, X. Wang, J. Chen, Y. Zhang, J. Pan, J. Xu, J. Zeng, Y. Wang, X. He, J. Huang, W. Zhao and J. B. Fan, *Nat. Commun.*, 2023, **14**, 5575.
18 B. Wang, B. Yin, Z. Zhang, Y. Yin, Y. Yang, H. Wang, T. P. Russell and S. Shi, *Angew. Chem., Int. Ed.*, 2022, **134**, e202114936.
19 Z. Yang, J. Wei, Y. I. Sobolev and B. A. Grzybowski, *Nature*, 2018, **553**, 313–318.

20 S. Shi, B. Qian, X. Wu, Z. Z. Yu and T. P. Russell, *Angew. Chem., Int. Ed.*, 2019, **58**, 18171–18176.
21 Y. Lin, H. Skaff, T. Emrick, A. D. Dinsmore and T. P. Russell, *Science*, 2003, **299**, 226–229.
22 Z. Cui, J. Zhang, Y. Xue and H. Duan, *Langmuir*, 2018, **34**, 3197–3206.
23 V. Garbin, J. C. Crocker and K. J. Stebe, *Langmuir*, 2012, **28**, 1663–1667.
24 F. Tu and D. Lee, *J. Am. Chem. Soc.*, 2014, **136**, 9999–10006.
25 J. Li, K. Li, Q. Zhang, L. Peng and X. Zhu, *Chem. Eng. J.*, 2025, **505**, 159361.
26 K. Yuan, Y. Zhang, Z. Yan, Q. Yun, T. Song, J. Guo, J. Feng, Z. Chen, X. Zhang, Z. Tang, W. Hu and T. Lu, *Angew. Chem., Int. Ed.*, 2025, e202421341.
27 A. Schrade, K. Landfester and U. Ziener, *Chem. Soc. Rev.*, 2013, **42**, 6823–6839.
28 B. Haney, D. Chen, L. H. Cai, D. Weitz and S. Ramakrishnan, *Langmuir*, 2019, **35**, 4693–4701.
29 X. Pei, Y. Tan, K. Xu, C. Liu, C. Lu and P. Wang, *Polym. Chem.*, 2016, **7**, 3325–3333.
30 B. P. Binks, *Curr. Opin. Colloid Interface Sci.*, 2002, **7**, 21–41.
31 F. Heidari-Dalfard, S. Tavasoli, E. Assadpour, R. Miller and S. M. Jafari, *Adv. Colloid Interface Sci.*, 2025, **336**, 103378.
32 W. Zhai, Y. Song, Z. Gao, J. B. Fan and S. Wang, *Macromolecules*, 2019, **52**, 3237–3243.
33 J. B. Fan, Y. Song, H. Liu, Z. Lu, F. Zhang, H. Liu, J. Meng, L. Gu, S. Wang and L. Jiang, *Sci. Adv.*, 2017, **3**, e1603203.
34 J. B. Fan, H. Liu, Y. Song, Z. Luo, Z. Lu and S. Wang, *Macromolecules*, 2018, **51**, 1591–1597.
35 B. P. Binks and P. D. I. Fletcher, *Langmuir*, 2001, **17**, 4708–4710.
36 T. Ondarçuhu, P. Fabre, E. Raphaël and M. Veyssié, *J. Phys.*, 1990, **51**, 1527–1536.
37 Y. Song, J. Zhou, J. B. Fan, W. Zhai, J. Meng and S. Wang, *Adv. Funct. Mater.*, 2018, **28**, 1802493.
38 S. Fujii, Y. Yokoyama, S. Nakayama, M. Ito, S. I. Yusa and Y. Nakamura, *Langmuir*, 2018, **34**, 933–942.
39 A. S. Parmar and M. Muschol, *J. Colloid Interface Sci.*, 2009, **339**, 243–248.
40 F. He, G. W. Becker, J. R. Litowski, L. O. Narhi, D. N. Brems and V. I. Razinkov, *Anal. Biochem.*, 2010, **399**, 141–143.
41 G. D. Goh, Y. L. Yap, S. Agarwala and W. Y. Yeong, *Adv. Mater. Technol.*, 2019, **4**, 1800271.
42 I. Bahnini, M. Rivette, A. Rechia, A. Siadat and A. Elmesbahi, *Int. J. Adv. Manuf. Technol.*, 2018, **97**, 147–161.

